ACS Catalysis

Research Article

pubs.acs.org/acscatalysis

Computational Insight into the Effect of Sn-Beta Na Exchange and Solvent on Glucose Isomerization and Epimerization

Jeffrey R. Christianson, Stavros Caratzoulas,* and Dionisios G. Vlachos

Catalysis Center for Energy Innovation and Department of Chemical and Biomolecular Engineering, University of Delaware, Newark, Delaware 19716, United States

Supporting Information

ABSTRACT: Sn-substituted zeolite Beta (Sn-Beta) is a promising catalyst for efficient aldose to ketose isomerization, a key step in the conversion of biomass to platform chemicals such as 5-(hydroxymethyl)furan and furfural. Recent experimental studies probing the mechanism and active site for glucose isomerization (to fructose) and competing epimerization (to mannose) have found that isomerization proceeds via a 1,2 intramolecular hydride transfer (HT) and epimerization by either two subsequent HT steps (on pure Sn-Beta; water and methanol) or one 1,2 intramolecular carbon shift (CS) step (on Na-exchanged Sn-Beta; water and methanol). In order to address remaining atomic-level mechanistic questions raised by this data, we investigate the various pathways with computational methods using several sizes of cluster models of Sn-Beta and density functional theory. First, we find an energetically plausible pathway for mannose formation via two subsequent HT steps that is consistent with experimental observations. Additionally, we conclude that Na exchange influences the mechanism by electrostatic stabilization of CS relative to HT and that this effect is relatively independent of geometric and flexibility constraints (even though the exact details of the mechanism are not). Finally, we find that the experimentally observed increase in glucose conversion when methanol is used as a solvent instead of water can be explained by the difference in solvation of the hydrophobic pores.

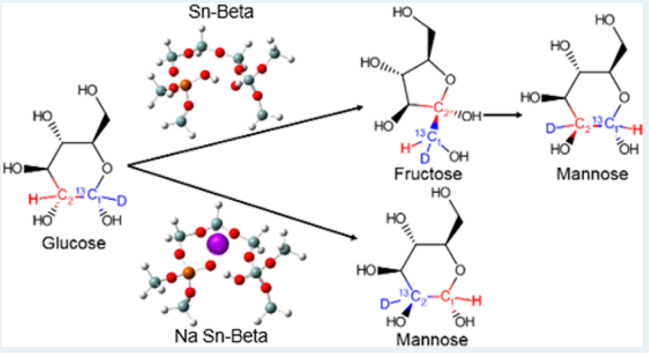

KEYWORDS: *heterogeneous catalysis, biomass, zeolite, hydride transfer, density functional theory*

INTRODUCTION

The utility of biomass as an alternative energy source depends critically on efficient conversion of raw plant matter to intermediate platform chemicals such as 5-(hydroxymethyl)-furan (HMF) or furfural, from which many useful chemicals and fuels can be produced.[1−4] Hydrolysis of cellulose yields monomers of glucose, but the subsequent dehydration to HMF is extremely inefficient. Because dehydration of fructose to HMF proceeds much more readily, there has been a renewed interest in isomerization of glucose to fructose. Although the enzymatic process for this transformation has been used commercially in the production of high fructose corn syrup for several decades,[5] new (and cheaper and/or regenerable) heterogeneous catalysts for this process are necessary for efficient biomass conversion to accommodate a wider range of temperatures and pH. To this end, Davis and co-workers have recently demonstrated that a large-pore, Sn-substituted zeolite (Sn-Beta) is a promising catalyst for glucose isomerization to fructose.[6] Not only is it active, but its stability at high temperatures and low pH allows for coupling of the isomerization with the subsequent dehydration of fructose to HMF in a "one-pot" (biphasic) transformation of glucose to HMF.[7]

Because of the importance of optimizing this step for efficient conversion of biomass to platform chemicals, the similarities to the enzymatic process, and the possibility of using Sn-Beta as a catalyst for other Lewis acid catalyzed reactions, the mechanism by which glucose isomerization occurs on Sn-Beta has received significant attention. In water, glucose must first be desolvated and diffuse into the hydrophobic pores of the zeolite; zeolites with hydrophilic pores (many defects) allow water uptake, but water adsorption to and extended hydrogen bonding networks around the Lewis acid Sn sites competitively inhibits binding and subsequent reaction of glucose.[8,9] In methanol, solvent uptake into the zeolite pores is observed but does not competitively inhibit catalyst activity;[8,9] in fact, activity is actually enhanced.[10] Upon diffusion into the pores, isotope labeling experiments have shown that adsorption of glucose to Sn-Beta facilitates ring opening (similar to the enzymatic process),[11] that the mechanism within the zeolite pores proceeds via an intramolecular hydride transfer (HT) from C2 to C1 (see Figure 1),[11−13] and that this HT is rate-limiting.[11,12] Additionally, glucose epimerization to mannose

Received: June 15, 2015
Revised: July 27, 2015
Published: July 30, 2015

DOI: 10.1021/acscatal.5b01258
ACS Catal. 2015, 5, 5256−5263

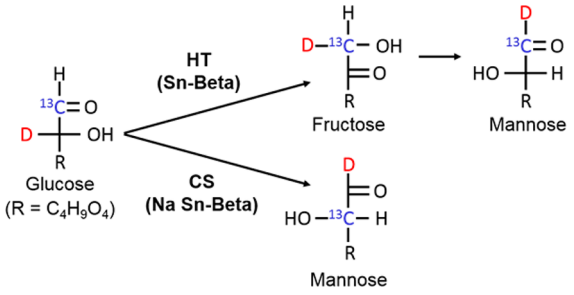

Figure 1. Fischer projection summary of hydride transfer (HT) and carbon shift (CS) pathways on Sn-Beta and Na-exchanged Sn-Beta, as elucidated from isotope-labeled experiments.[10]

via two subsequent intramolecular HTs (C2 to C1 followed by C1 to C2, see Figure 1) is also catalyzed by Sn-Beta and competes with isomerization.[10] Most recently, Davis and co-workers have conclusively demonstrated that it is the open Sn site (which includes a Sn−OH (stannanol) group formed from hydrolysis of a Sn−O−Si bond) that is active for both isomerization and epimerization by selective adsorption of NH_3 to the open sites (resulting in competitive inhibition of glucose binding) and by observing a mechanistic change upon Na-exchange of the adjacent Si−OH (silanol) proton.[10] Specifically, Na exchange favors epimerization by way of an intramolecular carbon shift (CS) from C2 to C1 (see Figure 1) over isomerization via HT.

Further insight into the mechanisms for glucose isomerization and epimerization has been elucidated from several computational investigations.[11,14−17] Despite large differences in the size of the model system for Sn-Beta, all agree (and/or assume) that isomerization occurs via the following steps (the first two of which have been confirmed by ^{13}C NMR experiments[11]): (1) closed-form glucose adsorption within the zeolite, (2) ring opening at the Sn site via cleavage of the C1−O−C5 hemiacetal bond, (3) deprotonation of the C2−OH, (4) C2 to C1 HT, (5) protonation of the fructose C1−O^-, (6) fructose ring closing, and (7) desorption. They also all report that HT is the step with by far the highest intrinsic activation energy, and there is a general consensus that the open Sn site is more active than the closed site. Rai et al.[15] and Li et al.[16] both propose participatory roles of adjacent silanol groups in stabilizing the HT step, consistent with the recent experimental observations with Na-exchanged Sn-Beta.[10] While the exact proposed mechanisms differ, in both cases, deprotonated C2−O^- binds to Sn and C1═O accepts a hydrogen bond from the adjacent silanol group; the silanol proton can then be transferred concertedly with the HT (so that steps 4 and 5 above occur simultaneously). Li et al.[17] also implicate this monodentate binding of glucose to Sn and a concerted mechanism, although the hydrogen bond is accepted from a protonated framework O (Si−O−Sn). Rai et al. further propose that the binding mode of the open glucose to Sn may affect the favored mechanism. While the monodentate binding is most stable (and HT most favorable), a bidentate binding mode involving both C2−O^- and C1═O coordination to Sn is also reported. In this case, the *intrinsic* barrier for CS is lower than that for HT, indicating that epimerization via CS may be more favorable if bidentate binding is stabilized.[15] However, authors employing larger Sn-Beta models (using quantum mechanical/molecular mechanical (QM/MM)[17] or periodic density functional theory (DFT)[14,16]) report that the open Sn site is not flexible enough to accommodate bidentate binding (unless a large "silanol nest" is introduced by completely removing a Si atom from the framework,[14] in which case the pore becomes much more hydrophilic and therefore much less active according to experimental results[8,9]).

In light of the most recent experimental data on Na-exchanged Sn-Beta,[10] several important mechanistic questions remain that have not been addressed by previous computational studies. First, how does the barrier for a second HT step from fructose to mannose compare to the barrier for the first HT step from glucose to fructose? Previous experiments indicated that mannose formation was only substantial in methanol and proceeded by a CS mechanism,[13] but this was later determined to be due to inadvertent K contamination;[10] isotope labeling then demonstrated that in samples without alkali-metal exchange the small amount of mannose that *is* produced is not formed by CS.[10] A pathway including a second HT from fructose to mannose is inferred from these experiments (and has been computationally proposed for xylose epimerization to lyxose[18]) but to the best of our knowledge has not been explicitly computed. Second, since it is the Na exchange, rather than the solvent, that changes the favored pathway to CS, what is the role of the Na in affecting the mechanism? Third, what *is* the role of the solvent? In particular, why does methanol increase glucose conversion compared to water?

In this manuscript, we report a computational study that addresses these three questions. We find that an energetically plausible pathway to form mannose by two HT steps exists, that the change in the electrostatic environment induced by Na exchange lowers the barrier to CS relative to HT, and that the presence of methanol in the hydrophobic pores of the zeolite likely accounts for the increased glucose conversion.

METHODS

Calculations were performed using the Gaussian 09 software package.[19] Sample input files for representative calculations, as well as geometries and free energies for each reported critical point, are provided in the Supporting Information. Two different Sn-Beta cluster models were used to compute reaction pathways for glucose isomerization and epimerization: (1) the model of Rai et al. with a total of 9 tetrahedral sites (9T cluster)[15] and (2) the 3-layered ONIOM H-Beta (polymorph A) cluster model of Patet et al. which treats 17 tetrahedral sites in the small layer, 17 additional tetrahedral sites in the intermediate layer, and 84 additional tetrahedral sites in the real layer (O-118T cluster).[20] The latter H-Beta model was converted to an open-site Sn-Beta model by making a Sn substitution for Si at a T-9 site (consistent with Rai et al.[15]) and hydrolyzing one of the Sn−O−Si bonds. Each model was used at a level of theory consistent with the original use by its developer. For the 9T cluster, the M06-2X hybrid meta-GGA functional[21] was used along with the LANL2DZP basis set and effective core potential (ECP) for Si and Sn atoms, the 6-31+G(d,p) basis set for H, C, O, and Na atoms, and the 6-31G basis set for the terminating H atoms (whose coordinates were always kept fixed). For the O-118T cluster, the small layer was treated with M06-2X in conjunction with the LANL2DZ basis set and ECP for Sn and the 6-31G(d,p) basis set for H, C, O, Na, and Si atoms. The intermediate layer was also treated with the M06-2X functional; however, the LANL2DZ basis set and ECP was used for both Si and Sn, and the 3-21G basis set was used for all other atoms. The real layer was described by the universal force field (UFF) molecular mechanics (MM) model,[22] and microiterations between the DFT and MM layers

DOI: 10.1021/acscatal.5b01258
ACS Catal. 2015, 5, 5256−5263

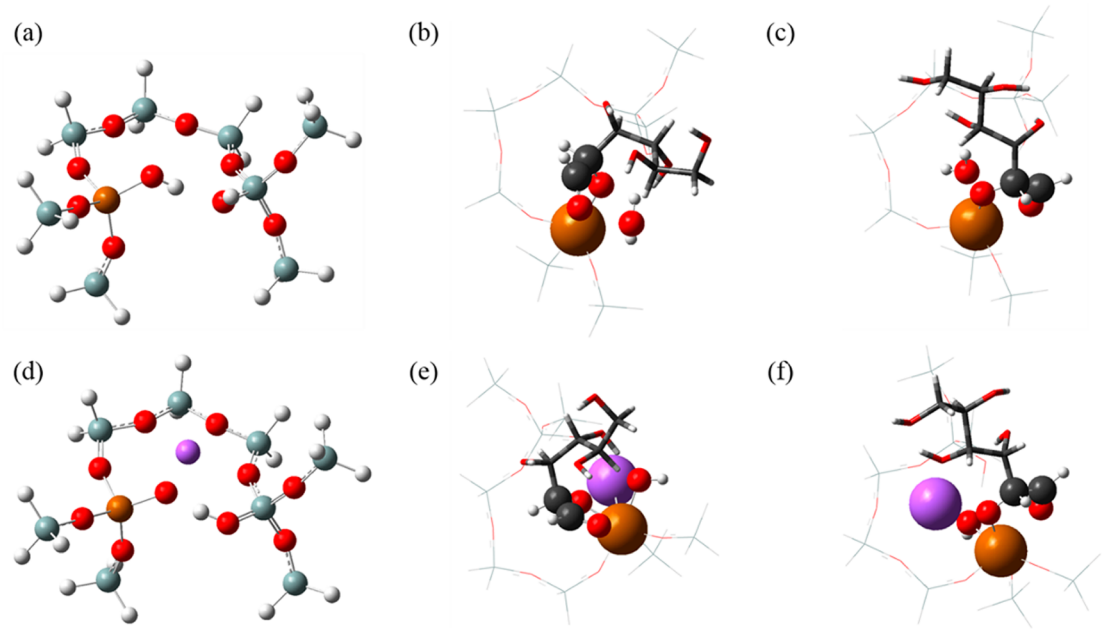

Figure 2. 9T-H (a–c) and 9T-Na (d–f) clusters. Shown for each are the bare cluster (a, d) and glucose adsorbed in the B1 (b, e) and B2 (c, f) bidentate binding modes. Atoms shown: H (white), O (red), Na (purple), Si (gray), Sn (brown). For clarity, multiple representations are used to show the two glucose bidentate binding modes: spheres proportional to atomic van der Waals radii for atoms near the Sn open site, tube frame for the rest of the glucose molecule, and wire frame for the rest of the cluster.

were turned off during geometry optimizations (in which only the small layer was relaxed while the intermediate and real layer atoms were frozen at their bulk crystallographic positions).

Using both models, we focus solely on the rate-limiting steps (HT or CS). While this precludes direct comparison of the computed intrinsic activation barriers to the experimentally observed apparent activation barriers, the goal of the present study is to understand experimental *trends* in pathway selectivity. We accomplish this by comparing to *trends* in the computed HT and CS pathways. Transition states (TS) were located by geometry scans and/or partial optimizations. The reactant (open, deprotonated glucose) was first optimized at a lower level of theory (a GGA functional and/or a smaller basis set). A series of partial optimizations were then performed that scanned over the angle that most appropriately described the reaction coordinate (i.e., the H–C2–C1 angle for HT and the C3–C2–C1 angle for CS). The geometry with the highest energy was then taken as a starting point for a TS optimization. Alternatively, the starting geometry for a TS search sometimes was taken from a partial optimization (holding the appropriate angle fixed) of a TS found previously that had been manually altered (e.g., rotating a sugar dihedral angle or replacing the silanol H atom with a Na atom). Once a TS was found at a low level of theory, that geometry was used as a starting point for a TS optimization at the level of theory reported above. The intrinsic reaction coordinate was then followed to find the minima connected by the TS, which were then optimized. All stationary points were verified as such by frequency calculations; minima contained zero imaginary frequencies and transition states (TS) contained exactly one imaginary frequency corresponding to the motion along the reaction coordinate. Frequency calculations were also used to add zero-point, enthalpy, and entropy corrections (at a temperature of 353 K, consistent with experimental conditions[10]), and the reaction pathways are reported as free energies at 353 K.

Solvent binding energies to Sn-Beta were calculated using the same ONIOM model described above but with basis sets and counterpoise corrections (using the H-terminated small layer to remove basis set superposition error) that have been recommended for accurately capturing binding trends.[20] For the small layer, the LANL2DZ basis set and ECP was used for Sn and the 6-311G(2df,p) basis set for H, C, O, and Si. In the intermediate layer, the LANL2DZ basis set and ECP was used for Sn and the 3-21G basis set for H, C, O, and Si. To crudely estimate the effect of solvation by methanol within the zeolite pore on the HT and CS mechanisms, a small $(H_3SiO)_3$-Sn–OH (4T) cluster was used to model the active site, and D-glyceraldehyde (a triose analogue of glucose) was adsorbed to the cluster. HT and CS TS's and minima were located (using the M06-2X functional, the LANL2DZ basis set and ECP for Sn, and the 6-311G(2df,p) basis set for H, C, O, and Si) both in the gas phase and in the presence of a methanol implicit solvation model based on the electron density of the solute (SMD).[23] The difference in the free energies of activation at 353 K between the gas-phase and implicit solvent systems was taken as an estimate for the stabilization of the HT or CS pathway in the methanol-rich zeolite pores.

RESULTS AND DISCUSSION

9T Cluster. The 9T cluster without Na exchange (9T-H) taken from Rai et al.[15] is shown in Figure 2a. Upon adsorption, ring opening, and deprotonation of glucose (to the Sn–OH, forming a water ligand), the bidentate binding mode reported by Rai et al. consists of the water ligand pointing out away from the cluster ring and the glucose C2–O^- occupying the Sn coordination site pointing in toward the ring (denoted here as B1, see Figure 2b). Here, we report a second bidentate binding mode which consists of the water ligand pointing in toward the cluster ring and the glucose C1–O occupying the Sn coordination site pointing out away from the ring (denoted as B2, see Figure 2c). Upon Na exchange (9T-Na), the most

DOI: 10.1021/acscatal.5b01258
ACS Catal. 2015, 5, 5256–5263

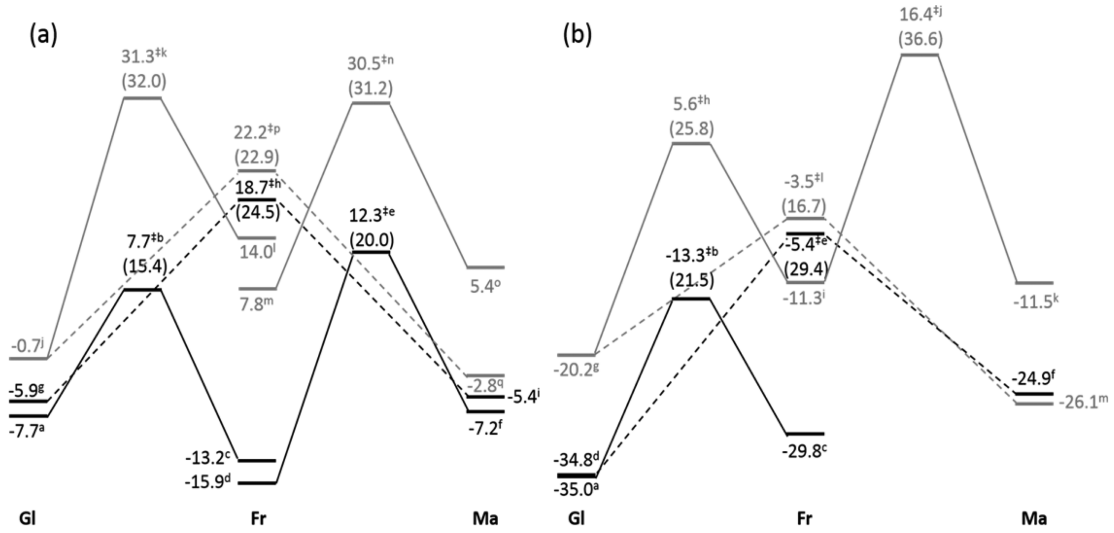

Figure 3. Calculated reaction pathways (kcal/mol) for HT (solid lines) and CS (dashed lines) from adsorbed, open, deprotonated glucose (Gl) to fructose (Fr) and/or mannose (Ma) on the 9T-H (a) and 9T-Na (b) cluster models. Pathways are shown for B1 (gray, see Figure 2b,e) and B2 (black, see Figure 2c,f) bidentate binding modes. Free energies are shown with respect to the isolated cluster and D-glucopyranose; numbers in parentheses indicate free energies of activation relative to Gl. Letters correspond to geometries supplied in the Supporting Information.

stable position of the Na ion (NPA elementary charge of +0.9) is found to be near the center of the cluster ring (see Figure 2d), optimizing electrostatic interactions with the surrounding framework O atoms (NPA elementary charges of approximately −1.4). Analogous to the 9T-H cluster, bidentate binding of open deprotonated glucose in both B1 (Figure 2e) and B2 (Figure 2f) modes is observed.

The computed reaction pathways on the 9T-H cluster are shown in Figure 3a. The CS and HT to fructose pathways for the B1 binding mode are the same as those reported by Rai et al.[15] (though reported here as free energies at 353 K), and the intrinsic barrier for CS is 9.1 kcal/mol lower than that for HT to fructose. However, the B2 binding mode is much more favorable; all points along the HT and CS pathways are much lower in energy than in the B1 binding mode. In contrast to the B1 mode, the CS TS is 11.0 kcal/mol higher in energy than the HT TS, indicating that bidentate binding does not inherently favor CS over HT. Additionally, the B2 binding mode pathways are more favorable than the monodentate (concerted) pathways reported by Rai et al.;[15] the HT to fructose TS is 10.9 kcal/mol lower in energy, and the CS TS is 3.5 kcal/mol lower in energy (see Supporting Information for pathway comparison). This indicates that bidentate binding may play an important role in HT versus CS pathways, but the qualitative conclusion remains the same for the 9T-H cluster, *namely, that HT is the preferred pathway in the absence of Na exchange*, which is consistent with the experimental observations.[10] Furthermore, the second HT from fructose to mannose has barriers relative to glucose that are comparable to those of the first HT from glucose to fructose. For the B1 mode, the second HT barrier is 0.8 kcal/mol lower than the first, and for the B2 mode, the second is 4.6 kcal/mol higher than the first. Thus, while the second HT will certainly compete with fructose ring closing and desorption (which will be in equilibrium with adsorbed fructose on the time scale of HT, since HT is the rate-limiting step), it is not surprising that small amounts of mannose formation by HT were observed in Sn-Beta without Na exchange.[10]

Since little to no HT occurs on Na-exchanged Sn-Beta (not even to fructose),[10] we focus on comparison between HT to fructose and CS to mannose on the 9T-Na cluster. In this case, it is important to note that monodentate binding analogous to that on the 9T-H cluster (C2−O^- bound to Sn and C1═O coordinating with Na) is not a feasible reaction pathway. This is because Na can only stabilize the product C1−O^- electrostatically and not through the formation of a covalent bond (such as the C1−O−H bond formed in the monodentate 9T-H pathway or the C1−O−Sn bond formed in the bidentate pathway). Thus, not only is glucose monodentate binding in this configuration not as stable as bidentate binding to Sn, but it also produces free energies of reaction and activation of 30−35 kcal/mol (see Supporting Information). Computed reaction pathways for bidentate binding on the 9T-Na cluster are shown in Figure 3b. The trends for B1 and B2 binding modes are qualitatively similar to those observed on the 9T-H cluster; B1 favors CS over HT, and B2 is energetically more stable and favors HT over CS. We note that this qualitative similarity is in spite of differences in how the Na interacts with the glucose backbone; the B2 binding allows for Na coordination with C3− and/or C4−OH groups, while B1 binding does not. This is also likely due to the fact that while Na certainly introduces an electrostatic field, it cannot create any geometric distortions in the glucose backbone via formation of covalent bonds. Despite the qualitative similarity with the 9T-H cluster, however, the quantitative difference between the CS TS and the HT TS decreases from 11.0 kcal/mol in the 9T-H cluster to 7.9 kcal/mol in the 9T-Na cluster. Therefore, the electrostatic presence of the Na appears to stabilize the CS TS more so than the HT TS. Although this observation does not capture the qualitative change from favoring HT to favoring CS observed experimentally, it does demonstrate a similar trend.

The conclusion that B2 binding (favoring HT) will dominate over B1 binding (favoring CS) is based on the relative binding energies of open deprotonated glucose. While medium-sized clusters can be effectively used to estimate reaction energetics which are mainly governed by local electronic effects,[24] relative binding energies may not be accurately captured due to the

DOI: 10.1021/acscatal.5b01258
ACS Catal. 2015, 5, 5256−5263

neglect of long-range electrostatic and confinement effects. For this reason, we also consider binding of glucose using a larger 3-layer zeolite Beta ONIOM cluster that has recently been benchmarked for adsorption energies.[20]

O-118T Cluster. An example configuration for open deprotonated glucose adsorbed on the ONIOM cluster with Na exchange (O-118T-Na cluster) is shown in Figure 4a. The most important feature of the O-118T cluster to note is the rigidity of the open Sn site in comparison to the 9T cluster. This is highlighted by a closer look at the hydrolyzed active site of the cluster without Na exchange (O-118T-H cluster, see Figure 4b). Instead of forming well-defined silanol and stannanol groups that are stabilized by hydrogen bonding to each other as in the 9T cluster (see Figure 2a), hydrolysis yields a sort of dibridging hydroxyl structure where each O atom occupies both a Si and a Sn coordination site (Sn−O distance of 2.0 Å, which is only slightly elongated from the closed site Sn−O distance of 1.8 Å). Upon deprotonation of glucose, one of the dibridging hydroxyls accepts the proton and becomes a water ligand coordinated to Sn; the other essentially becomes a protonated framework O, because it is still part of a Si−O−Sn bond. Thus, the open Sn site is already 5-fold coordinated, and monodentate binding of deprotonated glucose results in occupation of all six octahedral coordination sites on Sn. Due to steric considerations around the open Sn site, therefore, bidentate binding becomes nearly impossible. Indeed, multiple attempts to find such a binding mode failed. Only one bidentate mode was found when, during a geometry optimization with a monodentate-adsorbed glucose on the O-118T-H cluster, one of the dibridging hydroxyl protons migrated to an adjacent framework O, producing a silanol group opposite the water ligand and distinctly uncoordinated to Sn (Sn−O distance of 3.0 Å). From this geometry, a bidentate binding mode and HT and CS TS's were found but were much higher in energy than monodentate binding (which is discussed below), likely due to the resulting strain and steric effects. Moreover, upon Na exchange the Sn−O−Si bond re-forms and no bidentate binding is found on the O-118T-Na cluster. Further details regarding this possible bidentate binding mode are provided in the Supporting Information. In summary, the rigidity of the framework as modeled by the O-118T model appears to preclude a bidentate binding mode, which is consistent with previous computational investigations using QM/MM[17] or periodic DFT[14,16] Sn-Beta models.

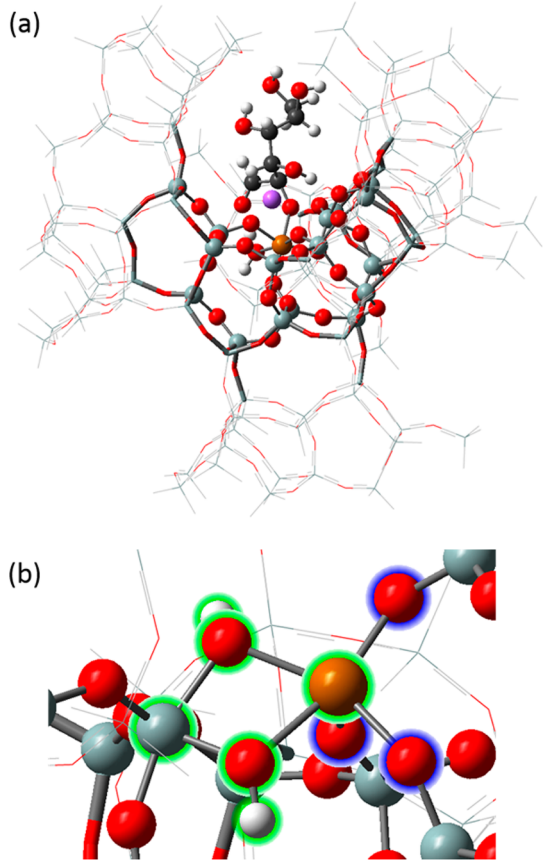

Figure 4. Na-exchanged O-118T cluster with glucose bound in a monodentate mode to the open Sn site (a), and a closer view of the O-118T cluster's hydrolyzed Sn−O−Si site (highlighted in green) and other framework O atoms coordinated to Sn (highlighted in blue) (b). Atoms shown: H (white), O (red), Na (purple), Si (gray), Sn (brown). The layers treated with high, medium, and low levels of theory are shown in ball-and-stick, tube frame, and wire frame representations, respectively.

Nevertheless, monodentate binding in which the C2−O$^-$ binds to Sn and the C1=O accepts a hydrogen bond from the Sn water ligand was found, and HT and CS reaction pathways from this binding were explored on both the O-118T-H and O-118T-Na clusters (see Figure 5). Since this model is significantly more computationally demanding than the 9T model, and since we have already confirmed the reasonability of a second HT from fructose to mannose, we consider only HT to fructose and CS to mannose on the O-118T clusters to explore the effect of Na exchange. For this monodentate binding the hydrogen bonding from the water ligand results in a concerted mechanism yielding the protonated product (fructose or mannose), similar to concerted mechanisms reported previously.[15−17] For the O-118T-H cluster (Figure 5a), the HT TS is 10.5 kcal/mol lower in energy than the CS TS. (It should be noted that for the CS, the saddle point optimization led to a TS connecting open *protonated* glucose and open protonated mannose; thus, it is still a concerted mechanism but with deprotonation from the glucose C2-OH instead of from a water ligand.) For the O-118T-Na cluster (Figure 5b), the HT TS is still lower in energy than the CS TS but only by 6.8 kcal/mol. Thus, as in the case of the 9T cluster, we again observe a shift toward stabilizing CS more than HT upon Na exchange, though not a qualitative change in the favored pathway.

Because this same trend is observed for two very different cluster models with two different binding modes (bidentate versus monodentate with a concerted reaction), it seems likely that the Na, rather than directly blocking the HT pathway, stabilizes (via the electrostatic field generated by its ionic nature) the CS TS more so than the HT TS. The failure to fully predict the change in favored pathway upon Na exchange may be due to the limitations of DFT. The M06-2X functional performs very well for barrier heights,[21,25] and our results are relatively insensitive to changing the functional to one parametrized to perform well for kinetics (MPW1K,[26,27] e.g., the difference between CS and HT transition states on the 9T-H cluster changes from 11.0 to 10.1 kcal/mol). However, errors of up to several kcal/mol should still be expected, and the possibility of larger errors should not be excluded due to the fact that exchange−correlation functional development necessarily contains an empirical component. Errors in trends, on the

DOI: 10.1021/acscatal.5b01258
ACS Catal. 2015, 5, 5256−5263

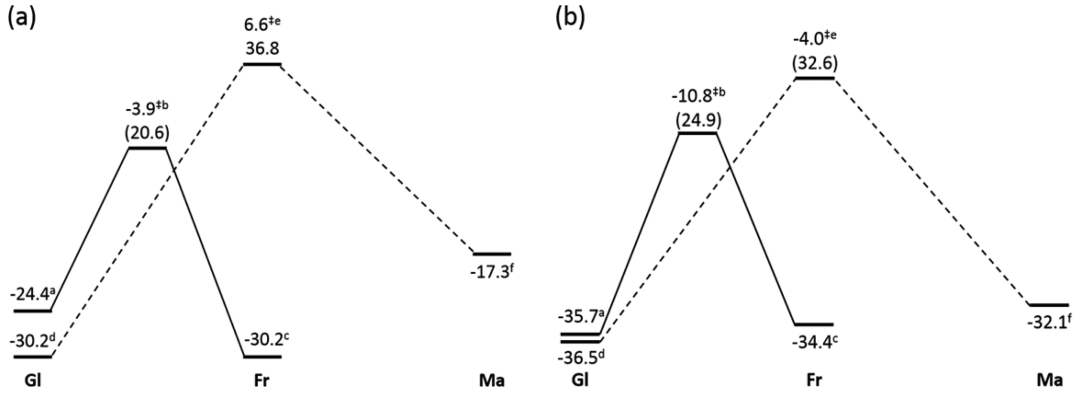

Figure 5. Calculated reaction pathways (kcal/mol) for HT (solid lines) and CS (dashed lines) from adsorbed, open, deprotonated glucose (Gl) to fructose (Fr) and/or mannose (Ma) on the O-118T-H (a) and O-118T-Na (b) clusters using the ONIOM model. Free energies are shown with respect to the isolated cluster and D-glucopyranose; numbers in parentheses indicate free energies of activation relative to Gl. Letters correspond to geometries supplied in the Supporting Information.

other hand, should be smaller due to cancellation of systematic DFT errors, and we believe that the *trend* exhibited for both of these cluster models captures the role of Na exchange on the mechanism.

Solvent Effects. Finally, we test the hypothesis that the enhanced glucose conversion in methanol compared to water is due to the vastly different pore solvation environment (i.e., the much greater uptake of methanol than water into the hydrophobic Sn-Beta pores[8,9]). Nuclear magnetic resonance (NMR) data that can be used to distinguish between tetrahedral and octahedral Sn coordination suggest that even when water is used as a solvent, a *small* amount of water is taken up into the hydrophobic pores and binds to the Sn sites.[8] Furthermore, Gounder et al. conjectured that the most abundant surface intermediate at steady state catalysis is two solvent molecules bound to Sn. Therefore, for either HT or CS in either water or methanol, the full catalytic cycle involves (1) desorption of the solvent, or Lewis base (B), molecules from the open Sn site (*), (2) adsorption/ring opening/deprotonation of glucose (G), (3) the rate-limiting step (HT or CS), and (4) protonation/ring closing/desorption of the product (P, fructose or mannose). This simplified mechanism proposed by Gounder et al.[8] (assuming steps (1), (2), and (4) are quasi-equilibrated) is depicted in Figure 6. Furthermore, in the

$$2B^* \overset{K_{1a}}{\rightleftharpoons} B(l) + B^* \overset{K_{1b}}{\rightleftharpoons} 2B(l) + *$$

$$G(l) + * \overset{K_2}{\rightleftharpoons} G^* \underset{k_{-3}}{\overset{k_3}{\rightleftharpoons}} P^* \overset{K_4}{\rightleftharpoons} P(l) + *$$

Figure 6. Mechanism for glucose isomerization (*P* = fructose) or epimerization (*P* = mannose), similar to the one proposed by Gounder et al.[8] Step 1: Solvent (B) desorption from the Sn open site. Step 2: Glucose (G) adsorption. Step 3: HT (fructose) or CS (mannose). Step 4: Product (P) desorption. K_i is the equilibrium constant for quasi-equilibrated state i; k_3 and k_{-3} are the forward and reverse rate constants for the rate-limiting step (HT or CS).

Supporting Information for their manuscript,[8] the authors show that under the assumptions of this model, the rate is determined by the following effective reaction:

$$G(l) + 2B^* \rightleftarrows \ddagger_3^* + 2B(l)$$

where $\ddagger_3^*$ is the transition state for step 3, and the rate is therefore proportional to

$$\text{rate} \propto \exp(-(\Delta G_{G(l)\rightarrow \ddagger_3^*} + \Delta G_{2B^*\rightarrow 2B(l)})/RT) = \exp(-\Delta G_{\text{eff}}/RT)$$

where ΔG_i is the free energy of process i, R is Boltzmann's constant in units of energy/(mol·K), and T is the temperature.

In light of our results presented above, it may only be necessary for one solvent molecule to desorb from the open Sn site. Bidentate binding may not be necessary if the concerted monodentate mechanism predominates, in which case Sn only needs one available coordination site to bind glucose. Additionally, if the O-118T cluster accurately captures the rigidity of the site, then hydrolysis of the Sn−O−Si bond changes the Sn coordination from four to five via the dibridging hydroxyl (Figure 4b). Octahedral coordination of the Sn open site would then occur with adsorption of just one solvent molecule; desorption of this one molecule could then be followed by monodentate binding of glucose and isomerization or epimerization as discussed above. For these reasons (and for simplicity), we assume desorption of only one solvent molecule in the analysis that follows. The effect of this assumption will be discussed following the analysis.

Proceeding with this assumption, the effective reaction simply becomes

$$G(l) + B^* \rightleftarrows \ddagger_3^* + B(l)$$

and the rate is proportional to

$$\text{rate} \propto \exp(-(\Delta G_{G(l)\rightarrow \ddagger_3^*} + \Delta G_{B^*\rightarrow B(l)})/RT) = \exp(-\Delta G'_{\text{eff}}/RT)$$

For the case of solvent-free pores, the free energy of the process $G(l) \rightarrow \ddagger_3^*$ is the sum of glucose desolvation ($G(l) \rightarrow G(g)$, $-\Delta G_{G,\text{solv}}$), glucose adsorption ($G(g) \rightarrow G^*$, $\Delta G_{G,\text{ads}}$), and activation to the rate-limiting (HT or CS) TS ($G^* \rightarrow \ddagger_3^*$, $\Delta G^{\ddagger}$). Additionally, the free energy of the process $B^* \rightarrow B(l)$ is the sum of solvent desorption ($B^* \rightarrow B(g)$, $-\Delta G_{B,\text{ads}}$) and solvent molecule solvation (i.e., the free energy of solvent condensation, $B(g) \rightarrow B(l)$, $-\Delta G_{\text{vap}}$). The ratio of the rate in methanol (m) to the rate in water (w) is proportional to

$$\frac{\text{rate}_m}{\text{rate}_w} \propto \exp(-(\Delta G'_{\text{eff,m}} - \Delta G'_{\text{eff,w}})/RT) = \exp(-\Delta\Delta G'_{\text{eff}}/RT)$$

It is this ratio that is of interest in comparing to experimental data. The experimentally observed glucose conversion is 2−10 times higher in methanol than in water[10] and corresponds to a

DOI: 10.1021/acscatal.5b01258
ACS Catal. 2015, 5, 5256−5263

$\Delta\Delta G_{eff}'$ of approximately −1 to −2 kcal/mol at 353 K, assuming that the data can be explained by a difference of the rates in the two solvents (which is a reasonable assumption, since experimental data taken after 10, 20, and 30 min show that the reaction is still progressing on this time scale and has not yet reached equilibrium). Continuing with the assumption of solvent-free pores (for both solvents), $\Delta\Delta G_{eff}'$ is given by

$$\Delta\Delta G_{eff}' = \Delta G_{G,solv,w} - \Delta G_{G,solv,m} + \Delta G_{B(w),ads} - \Delta G_{B(m),ads} + \Delta G_{vap,w} - \Delta G_{vap,m} = \Delta\Delta G_{G,solv} + \Delta\Delta G_{B,ads} + \Delta\Delta G_{vap}$$

because $\Delta G_{G,ads}$ and $\Delta G^{\ddagger}$ are independent of solvent, and these terms in methanol will cancel with the same terms in water. We estimate $\Delta\Delta G_{B,ads}$ (at 353 K) from calculated adsorption energies of water and methanol on the O-118T cluster to be +2.5 kcal/mol ($\Delta G_{B(w),ads}$ = −4.4 kcal/mol and $\Delta G_{B(m),ads}$ = −6.9 kcal/mol). This small difference slightly favoring methanol over water binding to the open Sn (Lewis acid) site is consistent with the small difference in Gutmann's Donor Number (a measure of the basicity of the solvent, 18 for water and 19 for methanol).[28] Both $\Delta\Delta G_{G,solv}$ and $\Delta\Delta G_{vap}$ at 353 K are estimated from experimental solubility[29−32] and thermochemical[33] data to be −2.6 kcal/mol and +1.1 kcal/mol, respectively (see Supporting Information for details). Thus, in the absence of pore solvation, we estimate $\Delta\Delta G_{eff}'$ to be +1.0 kcal/mol.

In the case of methanol, however, substantial solvation inside the zeolite pores will (1) decrease the glucose desolvation term due to partial solvation of the adsorbed sugar and (2) provide some stabilization of the rate-limiting TS, since both HT and CS involve charge redistribution from the C2−O$^-$ to the C1═O. We estimate the latter by the difference in activation free energy of HT (or CS) of D-glyceraldehyde on the 4T cluster model with and without the implicit SMD methanol solvation. This was done for HT bidentate, HT monodentate, CS bidentate, and CS monodentate bindings, and the free energies of activation were lower with SMD than without by 1.2, 1.5, 2.7, and 2.9 kcal/mol, respectively. These differences all lie in the range of 2.1 ± 0.9 kcal/mol, suggesting that changes between HT, CS, or binding mode are either small or not captured well by this crude approximation. (Although, we do note that there is a slight trend toward the electrostatic field of the implicit solvent stabilizing CS more so than HT and that this is consistent with our conclusions above concerning stabilization of CS due to the ionic nature of Na.) Thus, we estimate TS stabilization for HT/CS to be the center of this range, 2.1 kcal/mol. Adjusting for this stabilization, $\Delta\Delta G_{eff}'$ becomes −1.1 kcal/mol, indicating that the isomerization/epimerization will proceed more quickly in methanol. Estimating the partial solvation of the adsorbed glucose is not as straightforward but would be a fraction of the full solvation free energy (which can be estimated from experimental data to be −25 kcal/mol in water at 298 K[34] and therefore approximately −22 kcal/mol in methanol; see Supporting Information) and would only favor methanol even further. Regardless, based on this analysis, faster rates in methanol than in water may be expected, which is consistent with experimental observation.[10]

We note that this qualitative result is not largely affected when assuming that two (instead of one) solvent molecules must desorb from the active site. This may be estimated by addition of another $\Delta\Delta G_{B,ads}$ term (+2.5 kcal/mol) and another $\Delta\Delta G_{vap}$ term (+1.1 kcal/mol), which increases $\Delta\Delta G_{eff}'$ to +2.5 kcal/mol. This then predicts slightly slower rates in methanol than in water, but reasonable partial solvation of the adsorbed glucose in methanol should shift this once again in favor of methanol. Within the uncertainties of our approximations, this analysis supports our hypothesis that methanol increases glucose conversion relative to water simply due to its solvation of the hydrophobic Sn-Beta pores. It should be noted, though, that intermediate or transition state stabilization due to solvation within the zeolite pores is a secondary factor to any competitive inhibition such as binding to the active site. For example, the hydrophilic zeolites that allow significant uptake of water are inactive for glucose isomerization because the extended hydrogen bonding networks of Sn-adsorbed water, condensed water, and numerous silanol groups competitively inhibit glucose binding.[8,9] Thus, intermediate or transition state stabilization via solvation (which could be even more significant for water-filled versus methanol-filled pores due to water's high dielectric constant) becomes irrelevant. However, when comparing solvents for the active (hydrophobic-pore) Sn-Beta, competitive inhibition does not occur in either methanol (in which case glucose can competitively compete for binding to Sn sites) or water (essentially solvent-free pores). In this case, then, differences in solvation of the reaction pathway are likely to play an important role.

CONCLUSIONS

The computational results presented here shed new light on the mechanism for glucose isomerization and epimerization on Sn-Beta based on consideration of the most recent experimental data.[10] First, in the absence of Na exchange, we have reported an energetically plausible pathway for mannose formation by a second HT from fructose, consistent with isotope labeling experiments. Additionally, the similar qualitative trends exhibited by the 9T and O-118T clusters for different geometric and binding environments indicate that the role of Na exchange is to stabilize CS more so than HT due to its strong electrostatic presence. Furthermore, the differences between the 9T and O-118T clusters show that the exact structural details of the mechanism depend on the flexibility of the Sn open site within the zeolite framework. The more flexible active site of the 9T cluster allows for distinct and interacting silanol and stannanol groups upon Sn−O−Si hydrolysis, leaving tetrahedral Sn coordination. This, in turn, allows for bidentate binding of glucose to the open Sn site. However, the O-118T active site is much more rigid due to the extended framework. Hydrolysis of the Sn−O−Si bond yields 5-fold coordination of the open Sn site, which only allows for monodentate binding to Sn. Although the O-118T cluster may be considered a more realistic model because it incorporates more of the zeolite framework, zeolite flexibility[35,36] under reaction conditions could certainly affect the structure of the active site (though incorporating such effects is beyond the scope of the 0 K electronic structure calculations presented here). Nevertheless, the effect of Na on changing the mechanism appears to be independent of binding mode, because the same trends were observed for both clusters. Finally, we have shown that increased glucose conversion in methanol compared to water may be explained by the increased solvent uptake into the hydrophobic pores giving rise to partial solvation of the sugar−catalyst complex during reaction. In sum, the mechanistic insights reported here in conjunction with the most recent experimental results[10] provide a better understanding of glucose isomerization and competing

DOI: 10.1021/acscatal.5b01258
ACS Catal. 2015, 5, 5256−5263

epimerization on Sn-Beta that can inform further endeavors to streamline the process of biomass conversion to useful fuels and chemicals.

■ ASSOCIATED CONTENT

Supporting Information

The Supporting Information is available free of charge on the ACS Publications website at DOI: 10.1021/acscatal.5b01258.

A pdf file containing a comparison of 9T-H pathways to the concerted pathway reported by Rai et al.,[15] a presentation and discussion of 9T-Na pathways involving coordination of glucose to Na and of O-118T-H bidentate binding pathways, and an explanation of the estimation of $\Delta\Delta G_{G,solv}$ and $\Delta\Delta G_{vap}$ at 353 K from experimental data (PDF)

A zip file containing machine-readable example Gaussian 09 input files for representative calculations and all geometries and energies for reported minima and saddle points (ZIP)

■ AUTHOR INFORMATION

Corresponding Author

*E-mail: cstavros@udel.edu.

Notes

The authors declare no competing financial interest.

■ ACKNOWLEDGMENTS

This work was supported as part of the Catalysis Center for Energy Innovation, an Energy Frontier Research Center funded by the U.S. Department of Energy, Office of Science, Basic Energy Sciences under Award Number DE-SC0001004. Additional support was provided through the use of Information Technologies (IT) resources at the University of Delaware, specifically the high-performance computing resources. We thank Ryan E. Patet for providing optimized structures of the O-118T cluster model, Tyler R. Josephson, Dr. Sai Sriharsha M. Konda, Marat Orazov, and Kramer Brand for many useful discussions about this work, and Prof. Mark E. Davis for constructive feedback regarding this manuscript.

■ REFERENCES

(1) Van Putten, R. J.; Van Der Waal, J. C.; De Jong, E.; Rasrendra, C. B.; Heeres, H. J.; De Vries, J. G. *Chem. Rev.* **2013**, *113*, 1499−1597.

(2) Lange, J. P.; Van Der Heide, E.; Van Buijtenen, J.; Price, R. *ChemSusChem* **2012**, *5*, 150−166.

(3) Corma, A.; Iborra, S.; Velty, A. *Chem. Rev.* **2007**, *107*, 2411−2502.

(4) Wang, T.; Nolte, M. W.; Shanks, B. H. *Green Chem.* **2014**, *16*, 548−572.

(5) Bhosale, S. H.; Rao, M. B.; Deshpande, V. V. *Microbiol. Rev.* **1996**, *60*, 280−300.

(6) Moliner, M.; Román-Leshkov, Y.; Davis, M. E. *Proc. Natl. Acad. Sci. U. S. A.* **2010**, *107*, 6164−6168.

(7) Nikolla, E.; Román-Leshkov, Y.; Moliner, M.; Davis, M. E. *ACS Catal.* **2011**, *1*, 408−410.

(8) Gounder, R.; Davis, M. E. *J. Catal.* **2013**, *308*, 176−188.

(9) Gounder, R.; Davis, M. E. *AIChE J.* **2013**, *59*, 3349−3358.

(10) Bermejo-Deval, R.; Orazov, M.; Gounder, R.; Hwang, S.-J.; Davis, M. E. *ACS Catal.* **2014**, *4*, 2288−2297.

(11) Bermejo-Deval, R.; Assary, R. S.; Nikolla, E.; Moliner, M.; Román-Leshkov, Y.; Hwang, S.-J.; Palsdottir, A.; Silverman, D.; Lobo, R. F.; Curtiss, L. A.; Davis, M. E. *Proc. Natl. Acad. Sci. U. S. A.* **2012**, *109*, 9727−9732.

(12) Román-Leshkov, Y.; Moliner, M.; Labinger, J. A.; Davis, M. E. *Angew. Chem., Int. Ed.* **2010**, *49*, 8954−8957.

(13) Bermejo-Deval, R.; Gounder, R.; Davis, M. E. *ACS Catal.* **2012**, *2*, 2705−2713.

(14) Yang, G.; Pidko, E. A.; Hensen, E. J. M. *ChemSusChem* **2013**, *6*, 1688−1696.

(15) Rai, N.; Caratzoulas, S.; Vlachos, D. G. *ACS Catal.* **2013**, *3*, 2294−2298.

(16) Li, G.; Pidko, E. A.; Hensen, E. J. M. *Catal. Sci. Technol.* **2014**, *4*, 2241−2250.

(17) Li, Y.-P.; Head-Gordon, M.; Bell, A. T. *ACS Catal.* **2014**, *4*, 1537−1545.

(18) Choudhary, V.; Caratzoulas, S.; Vlachos, D. G. *Carbohydr. Res.* **2013**, *368*, 89−95.

(19) Frisch, M. J.; Trucks, G. W.; Schlegel, H. B.; Scuseria, G. E.; Robb, M. A.; Cheeseman, J. R.; Scalmani, G.; Barone, V.; Mennucci, B.; Petersson, G. A.; Nakatsuji, H.; Caricato, M.; Li, X.; Hratchian, H. P.; Izmaylov, A. F.; Bloino, J.; Zheng, G.; Sonnenberg, J. L.; Hada, M.; Ehara, M.; Toyota, K.; Fukuda, R.; Hasegawa, J.; Ishida, M.; Nakajima, T.; Honda, Y.; Kitao, O.; Nakai, H.; Vreven, T.; Montgomery Jr., J. A.; Peralta, J. E.; Ogliaro, F.; Bearpark, M.; Heyd, J. J.; Brothers, E.; Kudin, K. N.; Staroverov, V. N.; Kobayashi, R.; Normand, J.; Raghavachari, K.; Rendell, A.; Burant, J. C.; Iyengar, S. S.; Tomasi, J.; Cossi, M.; Rega, N.; Millam, J. M.; Klene, M.; Knox, J. E.; Cross, J. B.; Bakken, V.; Adamo, C.; Jaramillo, J.; Gomperts, R.; Stratmann, R. E.; Yazyev, O.; Austin, A. J.; Cammi, R.; Pomelli, C.; Ochterski, J. W.; Martin, R. L.; Morokuma, K.; Zakrzewski, V. G.; Voth, G. A.; Salvador, P.; Dannenberg, J. J.; Dapprich, S.; Daniels, A. D.; Farkas, Ö.; Foresman, J. B.; Ortiz, J. V.; Cioslowski, J.; Fox, D. J. *Gaussian 09*, Revisions A.02 and D.01; Gaussian, Inc.: Wallingford, CT, 2009.

(20) Patet, R. E.; Caratzoulas, S.; Vlachos, D. G. *J. Phys. Chem. C*; Unpublished work under review.

(21) Zhao, Y.; Truhlar, D. G. *Theor. Chem. Acc.* **2008**, *120*, 215−241.

(22) Rappe, A. K.; Casewit, C. J.; Colwell, K. S.; Goddard, W. A., III; Skiff, W. M. *J. Am. Chem. Soc.* **1992**, *114*, 10024−10035.

(23) Marenich, A. V.; Cramer, C. J.; Truhlar, D. G. *J. Phys. Chem. B* **2009**, *113*, 6378−6396.

(24) Fermann, J. T.; Moniz, T.; Kiowski, O.; McIntire, T. J.; Auerbach, S. M.; Vreven, T.; Frisch, M. J. *J. Chem. Theory Comput.* **2005**, *1*, 1232−1239.

(25) Linder, M.; Brinck, T. *Phys. Chem. Chem. Phys.* **2013**, *15*, 5108−5114.

(26) Lynch, B. J.; Fast, P. L.; Harris, M.; Truhlar, D. G. *J. Phys. Chem. A* **2000**, *104*, 4811−4815.

(27) Jones, G. O.; Guner, V. A.; Houk, K. N. *J. Phys. Chem. A* **2006**, *110*, 1216−1224.

(28) Mayer, U.; Gutmann, V.; Gerger, W. *Monatsh. Chem.* **1975**, *106*, 1235−1257.

(29) Thompson, J. D.; Cramer, C. J.; Truhlar, D. G. *J. Chem. Phys.* **2003**, *119*, 1661−1670.

(30) Peres, A.; Macedo, E. *Ind. Eng. Chem. Res.* **1997**, *36*, 2816−2820.

(31) Young, E. *J. Phys. Chem.* **1957**, *61*, 616−619.

(32) Montanes, F.; Olano, A.; Ibanez, E.; Fornari, T. *AIChE J.* **2007**, *53*, 2411−2418.

(33) Burgess, D. R. In *NIST Chemistry WebBook, NIST Standard Reference Database Number 69*; Linstrom, P. J.; Mallard, W. G., Eds.; National Institute of Standards and Technology: Gaithersburg MD, 20899.

(34) Geballe, M. T.; Skillman, A. G.; Nicholls, A.; Guthrie, J. P.; Taylor, P. J. *J. Comput.-Aided Mol. Des.* **2010**, *24*, 259−279.

(35) Sartbaeva, A.; Wells, S. A.; Treacy, M. M. J.; Thorpe, M. F. *Nat. Mater.* **2006**, *5*, 962−965.

(36) Kapko, V.; Dawson, C.; Treacy, M. M. J.; Thorpe, M. F. *Phys. Chem. Chem. Phys.* **2010**, *12*, 8531−8542.

DOI: 10.1021/acscatal.5b01258
ACS Catal. 2015, 5, 5256−5263